

Evolution of nonlinear Rossby waves in a dynamically time-dependent background flow via a quartic Korteweg-de Vries model

Shanshan Song(宋姗姗), Weiqi Zhang(张玮琦), Quansheng Liu(刘全生), Ruigang Zhang(张瑞岗)

Citation: Chin. Phys. B. 35, 094701 (2026). DOI: 10.1088/1674-1056/ae6567 | CSTR: 32038.14.CPB.ae6567
http://cpb.iphy.ac.cn; http://iopscience.iop.org/cpb

What follows is a list of articles you may be interested in

Time-resolved molecular non-equilibrium spectra in nanosecond laser induced air plasma

Xuteng Zhang(张续腾), Chaobo Yang(杨超博), Xun Yuan(袁勋), Minghong Han(韩明宏), Zhen Cao(曹振), Jiangbo Peng(彭江波), Xin Yu(于欣)

Chin. Phys. B. 34, 094701 (2025). DOI: 10.1088/1674-1056/ade24a | CSTR: 32038.14.CPB.ade24a

Neural network analysis for prediction of heat transfer of aqueous hybrid nanofluid flow in a variable porous space with varying film thickness over a stretched surface

Abeer S Alnahdi, Taza Gul

Chin. Phys. B. 34, 024701 (2025). DOI: 10.1088/1674-1056/ad989c | CSTR: 32038.14.CPB.ad989c

The interaction between zonal flow and Rossby waves with scalar nonlinearity

Zhang Xi-Ping(张喜平), Zhao Qiang(赵强)

Chin. Phys. B. 23, 064703 (2014). DOI: 10.1088/1674-1056/23/6/064703

SPECIAL TOPIC — Nonlinear localized waves: Theory, methods and applications

Evolution of nonlinear Rossby waves in a dynamically time-dependent background flow via a quartic Korteweg–de Vries model

Shanshan Song(宋姗姗)[1], Weiqi Zhang(张玮琦)[1], Quansheng Liu(刘全生)[1,2], and Ruigang Zhang(张瑞岗)[1,2,†]

[1] *School of Mathematical Sciences, Inner Mongolia University, Hohhot* 010030, *China*

[2] *Inner Mongolia Key Laboratory of Mathematical Modeling and Scientific Computing, Hohhot* 010030, *China*

(Received 18 February 2026; revised manuscript received 28 April 2026; accepted manuscript online 28 April 2026)

This study systematically investigates the evolution of nonlinear Rossby waves within a dynamically time-dependent background flow, based on the quasi-geostrophic potential vorticity equation under the beta-plane approximation. By employing the Gardner–Morikawa transformation and the multiple-scale perturbation method, a variable-coefficient quartic Korteweg–de Vries (vfqKdV) equation is derived to characterize the amplitude dynamics. By introducing a fractional linear transformation, the fifth-degree polynomial form of the first integral is reduced to the standard Weierstrass equation. Under the weak nonlinearity approximation, where the quartic nonlinear effect is relatively weak, we construct exact periodic traveling wave solutions. Applying the degeneracy condition $\Delta = 0$ further yields a solitary wave solution. This solution, obtained under the weak nonlinearity approximation, effectively captures the modulation of Rossby solitary waves by time-dependent background flows, providing a theoretical foundation for understanding the evolution of finite-amplitude Rossby waves in non-stationary geophysical flows.

Keywords: Rossby waves, time-dependent background flow, variable-coefficient quartic KdV equation, Weierstrass elliptic function

PACS: 47.11.St, 92.10.hf, 47.35.Fg

DOI: 10.1088/1674-1056/ae6567 **CSTR:** 32038.14.CPB.ae6567

1. Introduction

Rossby waves, fundamental large-scale wave phenomena in rotating fluid systems, owe their existence to the latitudinal gradient of the planetary Coriolis parameter, known as the beta-effect. First systematically described by Rossby,[1] these quasi-geostrophic waves play an indispensable role in governing atmospheric circulation patterns,[2] oceanic current systems, and climate variability mechanisms.[3] Linear theoretical frameworks have been highly successful in elucidating the dispersion relations and basic propagation characteristics of small-amplitude Rossby waves,[4,5] providing a solid foundation for subsequent research.

However, observations indicate that finite-amplitude Rossby waves are ubiquitous in nature, and their evolution involves complex nonlinear processes — such as wave–wave interactions,[6] energy dispersion, and the non-stationarity of the background flow[7] — that lie beyond the scope of linear theory. In realistic geophysical settings, background flows are intrinsically non-uniform and time-varying due to factors like seasonal forcing, topographic influences, and cross-scale energy transfer. This environmental non-stationarity profoundly modulates the propagation, stability, and energy localization of Rossby waves, giving rise to critical phenomena such as atmospheric blocking and anomalous waveguides.[8,9] Recent observational studies have further highlighted the importance of nonlinear wave-mean flow interactions in maintaining persistent weather patterns and triggering extreme climate events.[10]

To capture these nonlinear effects, increasingly sophisticated models have been developed. For instance, Zhang *et al.*[11] derived a nonlinear Schrödinger equation for wave packet evolution under topographic modulation, while Wang *et al.*[12] developed coupled Korteweg–de Vries (KdV) equations for barotropic–baroclinic interactions. Concurrently, variable-coefficient KdV equations, capable of reflecting spatial inhomogeneities such as latitudinal dependencies[13] and temporally evolving background flows,[14] have demonstrated unique advantages in describing Rossby wave dynamics, with associated theories and methods maturing progressively.[15,16] Regarding analytical techniques, classical frameworks like the inverse scattering transform,[17] Bäcklund transformations,[18] and Hirota's bilinear method[19] have been established for constant-coefficient integrable systems. For the more general variable-coefficient models, the Jacobi elliptic function expansion method[20,21] and multi-scale perturbation theory[22] offer flexible and effective analytical approaches. Beyond these analytical methods, data-driven techniques have recently gained attention for solving nonlinear wave equations. In particu-

[†]Corresponding author. E-mail: rgzhang@imu.edu.cn

© 2026 Chinese Physical Society and IOP Publishing Ltd. All rights, including for text and data mining, AI training, and similar technologies, are reserved.

lar, physics-informed neural networks (PINNs) have been successfully applied to investigate topographic Rossby solitary waves,[23] and related deep learning approaches have proven effective in predicting ultrafast soliton evolution in fiber lasers,[24,25] demonstrating the growing potential of machine learning in nonlinear wave dynamics. Meanwhile, for integrable systems characterized by higher-order Lax pairs, such as the Tzitzéica equation arising in affine differential geometry, the Riemann-Hilbert method has recently been employed to rigorously establish long-time asymptotic behaviors.[26]

Beyond geophysical fluid dynamics, solitary wave theory has found widespread applications across diverse physical systems. In magnetic materials, Jin *et al.*[27,28] constructed lump and rogue wave solutions for ferromagnetic systems, revealing the intricate interaction dynamics of localized magnetic excitations. These solutions exhibit transient localized structures with amplitudes that can grow rapidly and decay, characteristic of rogue wave phenomena. In contrast, the solitary wave derived in the present study corresponds to a steadily propagating, shape-preserving coherent structure arising from the balance between nonlinearity and dispersion in a time-dependent geophysical flow. While lump and rogue waves are typically associated with higher-order nonlinear interactions and appear as transient events, our solution represents a permanent-form wave that maintains its identity over long timescales under the weak nonlinearity approximation. In photonics, Mou *et al.*[29] investigated optical soliton formation in photonic Moiré lattices, demonstrating that the interplay between lattice geometry and nonlinearity gives rise to novel soliton propagation characteristics, while Si *et al.*[30] demonstrated the use of deep learning for dynamic modeling of vector-soliton pulsations in mode-locked fiber lasers. More recently, Wang *et al.*[31] harnessed cavitation-induced bubble collapse — a process bearing formal similarities to solitary wave dynamics — to launch millimeter-scale devices, achieving remarkable jumping heights and swimming speeds. These studies underscore the universality of solitary wave phenomena and suggest potential cross-disciplinary insights that may enrich the understanding of Rossby wave dynamics in geophysical contexts.

Despite these significant advances, existing models remain limited. Most are constrained by either constant-coefficient assumptions[11,12] or the inclusion of only lower-order nonlinearities,[32,33] failing to fully capture the non-autonomous nature induced by spatiotemporal variations in realistic flows and their coupling with higher-order nonlinearities. This limitation hinders our ability to accurately describe the amplitude evolution, morphological distortion, and energy exchange of Rossby waves in complex environments, such as rapidly changing flows or regions of strong nonlinearity. Moreover, the effects of dissipation and forcing, which are crucial in real geophysical systems,[34] are often neglected in these idealized models. Consequently, developing a model that incorporates both explicit time dependence and higher-order nonlinear terms is essential for deepening the understanding of nonlinear Rossby wave dynamics and enhancing predictive capabilities.

To address these challenges, this paper introduces a vfqKdV model. The main contributions of this work are threefold: Firstly, starting from the nonlinear quasi-geostrophic potential vorticity conservation equation and employing the Gardner–Morikawa transformation alongside multi-scale perturbation methods, we systematically derive a vfqKdV equation with explicit time-dependent coefficients, effectively generalizing traditional constant-coefficient or lower-order nonlinear models.[32,33] This derivation naturally incorporates the effects of a time-varying background flow, providing a more realistic framework for studying wave-mean flow interactions. Secondly, addressing the mathematical challenges posed by variable coefficients and the high-order nonlinearity, we implement an exact integration approach based on the Weierstrass elliptic function.[35,36] By introducing a fractional linear transformation, the fifth-degree polynomial form of the first integral is reduced to the standard Weierstrass equation. Under the weak nonlinearity approximation, where the quartic nonlinear effect is relatively weak (i.e., $|e_2| \ll 1$), we construct exact periodic traveling wave solutions. Applying the degeneracy condition $\Delta = 0$ further yields a solitary wave solution, which provides a theoretical basis for analyzing the modulation of Rossby solitary waves by time-dependent background flows. Lastly, through systematic numerical analysis and physical interpretation, we quantitatively elucidate how spatiotemporal variations in the background flow, mediated by the coefficients $e_i(t)$, modulate wave structure, amplitude, and propagation phase. Special attention is paid to the role of quartic nonlinearity in energy localization and the formation of coherent structures.[37] These findings offer insights that transcend the predictions of linear theory[4,5] and steady-state background assumptions.[8,9] The unified theoretical framework established in this study not only enriches the theoretical system of nonlinear wave dynamics but also provides new perspectives and quantitative tools for interpreting complex phenomena such as blocking events and eddy genesis in practical atmospheric and oceanic systems.[38,39]

2. Model derivations

Following the work of Hou *et al.*,[40] the quasi-geostrophic potential vorticity conservation equation under the β-plane approximation is adopted as

$$\left(\frac{\partial}{\partial t}+\frac{\partial \psi}{\partial x}\frac{\partial}{\partial y}-\frac{\partial \psi}{\partial y}\frac{\partial}{\partial x}\right)\left[\nabla^2\psi+\beta y+h(y)\right]=0, \quad (1)$$

where ψ represents the stream function, x and y denote the zonal and meridional coordinates, respectively, and the parameter β represents the gradient of the Coriolis parameter

with latitude, which is the fundamental physical cause of the existence and propagation of Rossby waves. $\nabla^2 = \partial^2/\partial x^2 + \partial^2/\partial y^2$ is the Laplace operator, and $h(y) = ly$ represents the topographic structure varying only along the meridional direction. This choice of $h(y)$ reflects a linearly sloping bottom, which is a common idealization in geophysical fluid dynamics to model large-scale topographic effects such as continental slopes or ocean ridges. The solution to Eq. (1) is required to fulfill the non-penetration boundary conditions of the sidewalls

$$\frac{\partial \psi}{\partial x} = 0, \quad y = 0, y_0, \tag{2}$$

where y_0 is the channel width.

The governing Eq. (1) is a prototypical nonlinear partial differential equation due to the advective term $\frac{\partial \psi}{\partial x}\frac{\partial}{\partial y} - \frac{\partial \psi}{\partial y}\frac{\partial}{\partial x}$, which represents the Jacobian determinant $J(\psi, \nabla^2\psi + \beta y + h(y))$ in vorticity dynamics. This nonlinear advection couples the stream function ψ with the potential vorticity $\nabla^2\psi + \beta y + h(y)$, enabling complex wave–wave and wave-mean flow interactions that are essential for capturing the formation of solitary waves, amplitude modulation, and other finite-amplitude effects beyond the reach of linear theory.

The stream function is defined as

$$\psi(x,y,t) = \psi_0(y,t) + \psi'(x,y,t), \tag{3}$$

where $\psi_0 = U_0(y) + \sum_{n=1}^{\infty} \varepsilon^n U_n(y,t)$ represents the time-dependent mean flow, which allows us to capture the effects of slowly varying background conditions, such as seasonal shifts or large-scale circulation changes, on the evolution of Rossby waves. And $\psi'(x,y,t) = \sum_{n=1}^{\infty} \varepsilon^n \psi_n'(x,y,t)$ denotes the disturbance component. The parameter ε is a small dimensionless quantity characterizing the amplitude ratio of the wave disturbance to the background flow, i.e., $\varepsilon \sim |\psi'|/|\psi_0| \ll 1$. This smallness assumption is physically justified for weakly nonlinear Rossby waves, where the wave amplitude is sufficiently small compared to the characteristic scale of the mean flow, allowing a systematic separation of scales via the Gardner–Morikawa transformation. For convenience, in the following text, $\psi'(x,y,t)$ will be denoted by $\psi(x,y,t)$ uniformly without any confusion.

Addressing the multiple scales and strong nonlinearity of large-scale atmospheric motions, the Gardner–Morikawa transformation is introduced $X = \varepsilon^{3/2}(x - c_0 t)$, $T = \varepsilon^{9/2} t$, where c_0 is the linear phase speed. This transformation effectively separates the fast and slow processes of wave evolution. Models of each order of perturbations are obtained according to systematic order-by-order perturbation analysis. At $O(\varepsilon^{5/2})$, an eigenvalue problem determining the fundamental mode structure is derived

$$\begin{cases} P(y)\dfrac{\partial \psi_1}{\partial X} - \left(c_0 + \dfrac{\mathrm{d}U_0}{\mathrm{d}y}\right)\dfrac{\partial^3 \psi_1}{\partial X \partial y^2} = 0, \\ \dfrac{\partial \psi_1}{\partial X} = 0, \quad y = 0, y_0, \end{cases} \tag{4}$$

where $P(y) = \dfrac{\mathrm{d}h}{\mathrm{d}y} + \beta + \dfrac{\mathrm{d}^3 U_0}{\mathrm{d}y^3}$.

The separable variable solution for ψ_1 is supposed to be

$$\psi_1 = A(X,T)G_1(y,T). \tag{5}$$

Substitution of Eq. (5) into Eq. (4) yields

$$\begin{cases} P(y)G_1 - \left(c_0 + \dfrac{\mathrm{d}U_0}{\mathrm{d}y}\right)\dfrac{\partial^2 G_1}{\partial y^2} = 0, \\ G_1(0) = G_1(y_0) = 0. \end{cases} \tag{6}$$

This constitutes a classical Sturm–Liouville eigenvalue problem for $G_1(y,T)$, which may be obtained through analytical or numerical methods. To fully characterize the evolution of the wave amplitude $A(X,T)$, it is necessary to address the higher-order problems.

For $O(\varepsilon^{7/2})$, we have

$$\begin{cases} P(y)\dfrac{\partial \psi_2}{\partial X} - \left(c_0 + \dfrac{\mathrm{d}U_0}{\mathrm{d}y}\right)\dfrac{\partial^3 \psi_2}{\partial X \partial y^2} \\ = -\dfrac{\partial \psi_1}{\partial X}\left(\dfrac{\partial^3 U_1}{\partial y^3} + \dfrac{\partial^3 \psi_1}{\partial y^3}\right) + \dfrac{\partial^3 \psi_1}{\partial X \partial y^2}\left(\dfrac{\partial U_1}{\partial y} + \dfrac{\partial \psi_1}{\partial y}\right), \\ \dfrac{\partial \psi_2}{\partial X} = 0, \quad y = 0, y_0. \end{cases} \tag{7}$$

Similarly, ψ_2 can be set as follows:

$$\psi_2 = A(X,T)G_{21}(y,T) + \frac{1}{2}A^2(X,T)G_{22}(y,T), \tag{8}$$

where $G_{21}(y,T)$ satisfies

$$\begin{cases} P(y)G_{21} - \left(c_0 + \dfrac{\mathrm{d}U_0}{\mathrm{d}y}\right)\dfrac{\partial^2 G_{21}}{\partial y^2} \\ = -G_1\dfrac{\partial^3 U_1}{\partial y^3} + \dfrac{\partial^2 G_1}{\partial y^2}\dfrac{\partial U_1}{\partial y}, \\ G_{21}(0) = G_{21}(y_0) = 0, \end{cases} \tag{9}$$

and $G_{22}(y,T)$ satisfies

$$\begin{cases} P(y)G_{22} - \left(c_0 + \dfrac{\mathrm{d}U_0}{\mathrm{d}y}\right)\dfrac{\partial^2 G_{22}}{\partial y^2} \\ = -G_1\dfrac{\partial^3 G_1}{\partial y^3} + \dfrac{\partial^2 G_1}{\partial y^2}\dfrac{\partial G_1}{\partial y}, \\ G_{22}(0) = G_{22}(y_0) = 0. \end{cases} \tag{10}$$

For $O(\varepsilon^{9/2})$, we similarly obtain

$$\begin{cases} P(y)\dfrac{\partial \psi_3}{\partial X} - \left(c_0 + \dfrac{\mathrm{d}U_0}{\mathrm{d}y}\right)\dfrac{\partial^3 \psi_3}{\partial X \partial y^2} \\ = -\dfrac{\partial}{\partial X}\left(\psi_1\dfrac{\partial^3 U_2}{\partial y^3} + \psi_2\dfrac{\partial^3 U_1}{\partial y^3} + \psi_1\dfrac{\partial^3 \psi_2}{\partial y^3} + \psi_2\dfrac{\partial^3 \psi_1}{\partial y^3}\right) \\ + \dfrac{\partial^3}{\partial X \partial y^2}\left(\psi_1\dfrac{\partial U_2}{\partial y} + \psi_2\dfrac{\partial U_1}{\partial y} + \psi_1\dfrac{\partial \psi_2}{\partial y} + \psi_2\dfrac{\partial \psi_1}{\partial y}\right), \\ \dfrac{\partial \psi_3}{\partial X} = 0, \quad y = 0, y_0. \end{cases} \tag{11}$$

A formal solution can also be readily obtained

$$\psi_3 = A(X,T)G_{31}(y,T)+\frac{1}{2}A^2(X,T)G_{32}(y,T) +\frac{1}{3}A^3(X,T)G_{33}(y,T), \tag{12}$$

where $G_{31}(y,T)$ satisfies

$$\begin{cases} P(y)G_{31}-\left(c_0+\dfrac{\mathrm{d}U_0}{\mathrm{d}y}\right)\dfrac{\partial^2 G_{31}}{\partial y^2}=-G_1\dfrac{\partial^3 U_2}{\partial y^3} \\ -G_{21}\dfrac{\partial^3 U_1}{\partial y^3}+\dfrac{\partial^2 G_1}{\partial y^2}\dfrac{\partial U_2}{\partial y}+\dfrac{\partial^2 G_{21}}{\partial y^2}\dfrac{\partial U_1}{\partial y}, \\ G_{31}(0)=G_{31}(y_0)=0, \end{cases} \tag{13}$$

and $G_{32}(y,T)$ satisfies

$$\begin{cases} P(y)G_{32}-\left(c_0+\dfrac{\mathrm{d}U_0}{\mathrm{d}y}\right)\dfrac{\partial^2 G_{32}}{\partial y^2}=-G_{22}\dfrac{\partial^3 U_1}{\partial y^3} \\ -G_1\dfrac{\partial^3 G_{21}}{\partial y^3}-G_{21}\dfrac{\partial^3 G_1}{\partial y^3}+\dfrac{\partial^2 G_{22}}{\partial y^2}\dfrac{\partial U_1}{\partial y} \\ +\dfrac{\partial^2 G_{11}}{\partial y^2}\dfrac{\partial G_{21}}{\partial y}+\dfrac{\partial^2 G_{21}}{\partial y^2}\dfrac{\partial G_1}{\partial y}, \\ G_{32}(0)=G_{32}(y_0)=0. \end{cases} \tag{14}$$

In the same way, $G_{33}(y,T)$ satisfies

$$\begin{cases} P(y)G_{33}-\left(c_0+\dfrac{\mathrm{d}U_0}{\mathrm{d}y}\right)\dfrac{\partial^2 G_{33}}{\partial y^2}=-\dfrac{1}{2}G_1\dfrac{\partial^3 G_{22}}{\partial y^3} \\ -G_{22}\dfrac{\partial^3 G_1}{\partial y^3}+\dfrac{1}{2}\dfrac{\partial^2 G_1}{\partial y^2}\dfrac{\partial G_{22}}{\partial y}+\dfrac{\partial^2 G_{22}}{\partial y^2}\dfrac{\partial G_1}{\partial y}, \\ G_{33}(0)=G_{33}(y_0)=0. \end{cases} \tag{15}$$

For $O(\varepsilon^{11/2})$, we have

$$\begin{cases} P(y)\dfrac{\partial\psi_4}{\partial X}-\left(c_0+\dfrac{\mathrm{d}U_0}{\mathrm{d}y}\right)\dfrac{\partial^3\psi_4}{\partial X\partial y^2}=-\dfrac{\partial\psi_1}{\partial X}\dfrac{\partial^3 U_3}{\partial y^3} \\ -\dfrac{\partial\psi_2}{\partial X}\dfrac{\partial^3 U_2}{\partial y^3}-\dfrac{\partial\psi_3}{\partial X}\dfrac{\partial^3 U_1}{\partial y^3}-\dfrac{\partial\psi_1}{\partial X}\dfrac{\partial^3\psi_3}{\partial y^3} \\ -\dfrac{\partial\psi_2}{\partial X}\dfrac{\partial^3\psi_2}{\partial y^3}-\dfrac{\partial^3\psi_3}{\partial X\partial y^2}\dfrac{\partial^3\psi_1}{\partial y^3}+\dfrac{\partial^3\psi_1}{\partial X\partial y^2}\dfrac{\partial U_3}{\partial y} \\ +\dfrac{\partial^3\psi_2}{\partial X\partial y^2}\dfrac{\partial U_2}{\partial y}+\dfrac{\partial^3\psi_3}{\partial X\partial y^2}\dfrac{\partial U_1}{\partial y}+\dfrac{\partial^3\psi_1}{\partial X\partial y^2}\dfrac{\partial\psi_3}{\partial y} \\ +\dfrac{\partial^3\psi_2}{\partial X\partial y^2}\dfrac{\partial\psi_2}{\partial y}+\dfrac{\partial^3\psi_3}{\partial X\partial y^2}\dfrac{\partial\psi_1}{\partial y}-\dfrac{\partial^3 U_1}{\partial T\partial y^2} \\ -\dfrac{\partial^3\psi_1}{\partial T\partial y^2}+\dfrac{\partial U_0}{\partial y}\dfrac{\partial^3\psi_1}{\partial X^3}, \\ \dfrac{\partial\psi_3}{\partial X}=0, \quad y=0,y_0. \end{cases} \tag{16}$$

To ensure the non-singularity of the perturbation solution, the solvability condition of the multiple-scale perturbation method is applied. By setting $\psi_4=0$ and substituting the expressions for ψ_1, ψ_2, and ψ_3 into Eq. (16), the secular terms are eliminated after integrating over $y\in[0,y_0]$. This yields the vfqKdV equation

$$\frac{\partial A}{\partial T}+e_1\frac{\partial^3 A}{\partial X^3}+e_2A^3\frac{\partial A}{\partial X}+e_3A^2\frac{\partial A}{\partial X} +e_4A\frac{\partial A}{\partial X}+e_5\frac{\partial A}{\partial X}+e_6A+e_7=0, \tag{17}$$

with $e_1=\frac{I_1}{I_0},e_2=\frac{I_2}{I_0},e_3=\frac{I_3}{I_0},e_4=\frac{I_4}{I_0},e_5=\frac{I_5}{I_0},e_6=\frac{I_6}{I_0},e_7=\frac{I_7}{I_0}$, where I_i $(i=0,1,\ldots,7)$ are shown in the Appendix. This equation generalizes the classical KdV equation by including higher-order nonlinear terms and time-dependent coefficients, which capture the effects of a slowly varying background environment. Physically, the coefficients $e_i(T)$ encapsulate the influence of the time-dependent background flow on the evolution of Rossby waves. Specifically, $e_1(T)$ represents the linear dispersion effect, which governs the spreading of wave packets. The terms $e_2(T)$, $e_3(T)$, and $e_4(T)$ correspond to the quartic, cubic, and quadratic nonlinearities, respectively, reflecting the hierarchical structure of wave-mean flow interactions at different levels of nonlinear intensity. The coefficient $e_5(T)$ arises from the advective transport of the wave by the background flow, while $e_6(T)$ and $e_7(T)$ characterize linear absorption/amplification and external forcing effects, respectively. The time dependence of these coefficients originates from the temporal variations of the background flow, such as seasonal modulation or large-scale circulation changes, thereby enabling the model to capture the non-autonomous nature of realistic geophysical environments.

3. Solution for vfqKDV

To facilitate analytical progress while retaining physical relevance, we consider a specific form of the background flow that allows for an explicit solution to the eigenvalue problem

$$U_0(y)=b_0\sin\left(\frac{\pi y}{y_0}\right)-b_1y,$$
$$U_1(y,t)=a_1\cdot y^2+a_2(t)\cdot y+a_3(t),\ \ U_n=0,\ \ (n\geq 2), \tag{18}$$

where $U_0(y)$ represents the leading-order barotropic background flow. The parameter b_0 controls the amplitude of the sinusoidal component, which captures a basic zonal flow with a single meridional mode. The parameter b_1 controls the strength of the uniform zonal advection, since the associated zonal velocity is $-\mathrm{d}U_0/\mathrm{d}y=b_1$, a constant. The first-order correction $U_1(y,t)$, of order ε relative to U_0, accounts for slow temporal variations induced by external factors such as seasonal forcing. The parameter a_1 determines the meridional curvature of the background streamfunction, corresponding to a linearly sheared zonal flow with constant shear $-2a_1$. The time-dependent coefficients $a_2(t)$ and $a_3(t)$ represent a slowly varying linear shear and a uniform background shift, respectively. The condition $U_n=0$ for $n\geq 2$ is a simplification that ensures a closed-form solution while preserving the essential physics of a slowly evolving background. This construction

guarantees an explicit eigenfunction $G_1(y,T)$ and provides a mathematically tractable framework for deriving the variable-coefficient quartic KdV equation. Physically, this configuration corresponds to a base flow with a sinusoidal horizontal structure, superimposed with a temporally evolving quadratic perturbation, effectively capturing the slow variations in realistic atmospheric or oceanic flows induced by seasonal forcing, topographic effects, or energy cascade processes

$$\psi_0 = b_0 \sin\left(\frac{\pi y}{y_0}\right) - b_1 y + \varepsilon(a_1 \cdot y^2 + a_2(t)\cdot y + a_3(t)). \quad (19)$$

This specific form of ψ_0 allows the eigenvalue problem (6) to be solved explicitly. The spatial structure of the primary flow conforms to the channel geometry and satisfies the impermeability boundary conditions. Under the given boundary conditions $G_1(0) = G_1(y_0) = 0$, the leading-order eigenfunction for the wave perturbation is identified as the fundamental sinusoidal mode

$$G_1(y,T) = \sin\left(\frac{\pi y}{y_0}\right). \quad (20)$$

To solve the variable-coefficient Eq. (17) governing the evolution of nonlinear Rossby waves, a traveling wave transformation incorporating a slowly varying frequency is introduced, taking into account the slowly varying nature of the background flow

$$A(X,T) = \phi(\zeta), \quad \zeta = kX + \int \Omega(T)\,\mathrm{d}T, \quad (21)$$

where ϕ is a function representing the traveling wave shape, k is a constant wavenumber, and $\Omega(T)$ is an undetermined slowly varying frequency function, whose time dependence reflects the modulation of the wave propagation phase speed by the non-stationarity of the background flow. Substituting Eq. (21) into Eq. (17) and utilizing the solvability condition $e_7(T) = 0$ yields

$$\begin{aligned}&\Omega(T)\phi' + e_1(T)k^3\phi''' + e_2(T)k\phi^3\phi' + e_3(T)k\phi^2\phi' \\ &+ e_4(T)k\phi\phi' + e_5(T)k\phi' + e_6(T)\phi = 0, \end{aligned} \quad (22)$$

where the prime denotes differentiation with respect to ζ. In Eq. (22), the term $\Omega\phi'$ characterizes the correction to the local wave frequency induced by the slowly varying background; $e_1k^3\phi'''$ represents the linear dispersion term governing the spatial spreading of the wave packet; the terms $e_2\phi^3\phi'$, $e_3\phi^2\phi'$, and $e_4\phi\phi'$ correspond to the quartic, cubic, and quadratic nonlinearities, respectively, reflecting the hierarchical structure of wave–mean flow interactions at different levels of nonlinear intensity; the term $e_5k\phi'$ originates from the advective transport of the wave by the background flow; and the term $e_6\phi$ characterizes the linear absorption or amplification of wave energy by the background flow.

Since the large-scale evolution of the background flow is much slower than the phase variation of the Rossby wave, the coefficients $e_i(T)$ and $\Omega(T)$ can be treated as locally constant at any fixed slow time T. This "frozen coefficient" approximation is widely adopted in the study of wave propagation in non-stationary media,[41] based on the fact that the characteristic time scale of the background variation is significantly longer than the wave period. Consequently, Eq. (22) reduces to a local constant-coefficient ordinary differential equation

$$a\phi''' + b\phi^3\phi' + c\phi^2\phi' + d\phi\phi' + f\phi' + g\phi = 0, \quad (23)$$

with $a = e_1k^3, b = e_2k, c = e_3k, d = e_4k, f = \Omega + e_5k, g = e_6$.

It can be rigorously verified from the integral expressions provided in the Appendix that $e_6(T) = 0$, i.e., $g = 0$. This condition indicates that, within the solvability framework of the multiple-scale perturbation analysis, the linear absorption of wave energy by the background flow is precisely balanced by higher-order nonlinear interactions, thereby ensuring energy conservation of the wave–mean flow system at the leading order. This property is intimately related to the physical mechanism that sustains the structural stability of solitary waves in non-stationary media.

Under the condition $g = 0$, integrating Eq. (23) once with respect to ζ yields

$$\frac{a}{2}(\phi')^2 + \frac{b}{20}\phi^5 + \frac{c}{12}\phi^4 + \frac{d}{6}\phi^3 + \frac{f}{2}\phi^2 - G_1\phi = G_2, \quad (24)$$

where G_1 and G_2 are integration constants. The first term on the left-hand side of Eq. (24) corresponds to the "kinetic energy" of the wave profile, while the remaining four terms constitute the "potential energy" function. The linear and constant terms on the right-hand side reflect the conservation of the total "mechanical energy" of the system. This energy conservation structure is characteristic of Hamiltonian systems and serves as the mathematical foundation for the long-term stability of solitary waves.

Rearranging Eq. (24) leads to the standard form of the first integral

$$(\phi')^2 = A_5\phi^5 + A_4\phi^4 + A_3\phi^3 + A_2\phi^2 + A_1\phi + A_0, \quad (25)$$

where the coefficients are related to the original physical parameters by $A_5 = -\frac{e_2}{10e_1k^2}$, $A_4 = -\frac{e_3}{6e_1k^2}$, $A_3 = -\frac{e_4}{3e_1k^2}$, $A_2 = -\frac{\Omega+e_5k}{e_1k^3}$, $A_1 = \frac{2G_1}{e_1k^3}$, and $A_0 = \frac{2G_2}{e_1k^3}$. After obtaining the first integral form of Eq. (25), $(\phi')^2 = P_5(\phi)$, we are faced with a nonlinear oscillation problem involving a fifth-degree polynomial. From the theory of ordinary differential equations, it is known that for all equations of the form $(y')^2 = \sum_{k=0}^{n} a_k y^k$, when the right-hand side is a polynomial of degree not less than three, their bounded solutions can usually be expressed by elliptic functions. This conclusion originates from the classical studies on elliptic integrals and elliptic functions in the 19th century and has been systematically summarized in various standard textbooks.[42]

In particular, for cubic and quartic polynomials, the solutions can be directly given by Jacobi or Weierstrass elliptic

functions; for polynomials of degree five and higher (forming hyperelliptic curves), they can be reduced to solvable forms through birational transformations. A universal and effective method is to introduce a fractional linear transformation that maps the original variable to a new variable, thereby reducing the equation to the standard Weierstrass equation $(u')^2 = 4u^3 - g_2u - g_3$. The effectiveness of this method and its application in nonlinear wave equations can be found in authoritative works such as Byrd.[36]

In view of the structure of $P_5(\phi)$ in this equation, which in general contains a quintic term characterized by A_5, direct application of the Jacobi elliptic function expansion method would encounter fundamental difficulties, as the balance law leads to non-integer powers. Even under the weak nonlinearity approximation where $|e_2| \ll 1$, the presence of the quintic term necessitates a more systematic approach. Therefore, this paper adopts the above-mentioned exact solution method based on the Weierstrass elliptic function $\wp$.

Accordingly, the exact traveling wave solution of Eq. (25) is assumed to take the form

$$\phi(\zeta) = \frac{\alpha\wp(\zeta-\zeta_0)+\beta}{\gamma\wp(\zeta-\zeta_0)+1}, \tag{26}$$

where $\alpha(T)$, $\beta(T)$, and $\gamma(T)$ are undetermined time-varying parameters, $\wp(\zeta) = \wp(\zeta; g_2, g_3)$ is the Weierstrass elliptic function, $g_2(T)$ and $g_3(T)$ are Weierstrass invariants that are also undetermined, and ζ_0 is a phase constant. The rationale for this assumed form is that it is precisely the direct embodiment of the aforementioned fractional linear transformation and is sufficient to capture the elliptic function solution structure of the algebraic curve defined by the fifth-degree polynomial.

Let $W = \wp(\zeta-\zeta_0)$, then $\phi = \frac{\alpha W+\beta}{\gamma W+1}$. Furthermore, the Weierstrass elliptic function satisfies

$$(W')^2 = 4W^3 - g_2W - g_3, \tag{27}$$

and substituting into the equation for $\phi(\zeta)$, we obtain

$$\begin{aligned}&(\alpha-\beta\gamma)^2(4W^3-g_2W-g_3)(\gamma W+1)\\ &= C_5W^5+C_4W^4+C_3W^3+C_2W^2+C_1W+C_0,\end{aligned} \tag{28}$$

where C_i $(i = 0,1,2,3,4,5)$ are shown in the Appendix.

Then, according to the coefficient correspondence rule, we can obtain the following expression:

$$\begin{cases} 0 = C_5, \\ 4(\alpha-\beta\gamma)^2\gamma = C_4, \\ 4(\alpha-\beta\gamma)^2 = C_3, \\ -(\alpha-\beta\gamma)^2 g_2\gamma = C_2, \\ -(\alpha-\beta\gamma)^2(g_2+g_3\gamma) = C_1, \\ -(\alpha-\beta\gamma)^2 g_3 = C_0. \end{cases} \tag{29}$$

The assumption that $\gamma = 0$ leads to a trivial solution. Therefore, $\gamma \neq 0$. We then consider another classical assumption: the solution is assumed to be the reciprocal of a function of $\wp$, that is, $\alpha = 0$. Equation (29) can then be solved as

$$\begin{cases} G_2 = 0, \\ \gamma(T) = \dfrac{12e_1(T)k^3}{\Omega(T)+e_5(T)k}, \\ \beta(T) = \dfrac{6G_1}{\Omega(T)+e_5(T)k}, \\ g_2(T) = \dfrac{G_1e_4(T)}{6e_1(T)^2k^5} + \dfrac{[\Omega(T)+e_5(T)k]^2}{12e_1(T)^2k^6}, \\ g_3(T) = \dfrac{3e_2(T)G_1^3}{20e_1(T)^3k^8[\Omega(T)+e_5(T)k]} + \dfrac{e_3(T)G_1^2}{24e_1(T)^3k^8} \\ \quad \times \dfrac{e_4(T)G_1[\Omega(T)+e_5(T)k]}{72e_1(T)^3k^8} \times \dfrac{[\Omega(T)+e_5(T)k]^3}{216e_1(T)^3k^9}, \end{cases} \tag{30}$$

under the special solution condition $\alpha = 0$. Substituting the parameters $\gamma(T)$ and $\beta(T)$ determined by Eq. (30), together with the Weierstrass invariants $g_2(T)$ and $g_3(T)$, into the transformation relation Eq. (26), and combining it with the definition of the Weierstrass elliptic function $\phi(\zeta) = \wp(\zeta - \zeta_0; g_2, g_3)$, we obtain the explicit expression of the wave function $\phi(\zeta)$. Furthermore, using the correspondence between the amplitude function $A(X,T)$ and $\phi(\zeta)$, and substituting back into the original traveling-wave variable $\zeta = kX + \int \Omega(T)\,\mathrm{d}T$, we obtain the periodic wave solution in the following form:

$$\begin{aligned}A(X,T) = 6G_1\Bigg[12e_1k^3\cdot\wp\Big(kX+\int\Omega(T)\,\mathrm{d}T\\ -\zeta_0; g_2(T), g_3(T)\Big)+\Omega(T)+e_5k\Bigg]^{-1},\end{aligned} \tag{31}$$

where $\wp(\cdot; g_2, g_3)$ is the Weierstrass elliptic function. This solution explicitly characterizes the periodic evolution of the nonlinear Rossby wave amplitude under the modulation of the time-varying background flow, whose structure is jointly determined by the background flow parameters $e_i(T)$ and the integration constant G_1.

It is worth noting that the above solution (31) is derived under the simplifying assumption $\alpha = 0$. Mathematically, this assumption imposes the constraint $e_2 = 0$. From a physical perspective, however, this simplification corresponds to the case where the quartic nonlinear effect is relatively weak (i.e., $|e_2| \ll 1$). Specifically, when the Rossby wave amplitude is sufficiently small, the background shear is weak, or the topographic variations are gentle, the quartic nonlinear term $e_2A^3A_X$ can be treated as a higher-order small quantity compared to the cubic and quadratic nonlinear terms. Under this weak nonlinearity approximation, the original variable-coefficient quartic KdV equation reduces to a variable-coefficient cubic KdV model, and solution (31) represents an exact periodic solution of this reduced model.

Despite the adoption of this weak nonlinearity approximation, solution (31) effectively captures the essential modulation of Rossby wave propagation by time-dependent background flows. To obtain a solitary wave solution, we further apply the degeneracy condition $\Delta = 0$ of the Weierstrass elliptic function. This degeneration process transforms the periodic solution into a localized solitary wave form. The resulting solitary wave solution, obtained under the weak nonlinearity approximation, corresponds to the variable-coefficient cubic KdV model and provides valuable insight into the structural stability and parameter sensitivity of Rossby solitary waves under slowly varying background conditions.

Let $z = \zeta - \zeta_0$. The emergence of the solitary wave solution is fundamentally rooted in the singular degeneration of the Weierstrass elliptic function $\wp(z)$. According to the authoritative handbook by Abramowitz and Stegun,[43] specifically in the discussion of degenerate cases, the doubly periodic nature of the function collapses when the discriminant vanishes, i.e., $\Delta = g_2^3 - 27g_3^2 = 0$.

Geometrically, this condition implies that the underlying elliptic curve degenerates from a torus (genus 1) into a rational curve with a nodal singularity. Analytically, the characteristic cubic equation $4t^3 - g_2 t - g_3 = 0$ possesses a repeated root. Let e_0 be the repeated root; given the relation $\sum e_i = 0$ for the Weierstrass form, the distinct root must be $-2e_0$. Consequently, the fundamental differential equation for $\wp(z)$ simplifies to

$$(\wp')^2 = 4(\wp + 2e_0)(\wp - e_0)^2.$$

By separating variables and integrating, or by applying the transformation provided in Ref. [43], the elliptic function degenerates into the following hyperbolic form:

$$\wp(z) = e_0 + \frac{3e_0}{\sinh^2(\sqrt{3e_0}z)}, \tag{32}$$

where it is required that $e_0 > 0$ to ensure that the expression inside the square root is positive. Here, κ is the soliton width parameter. Assuming $\kappa = \sqrt{3e_0}$ gives $\wp(z) = e_0 + \dfrac{\kappa^2}{\sinh^2(\kappa z)}$. In the context of nonlinear wave dynamics, this limit represents the scenario where the period of cnoidal waves tends to infinity, effectively resulting in a localized solitary wave or soliton solution.

Substituting the degenerate form Eq. (32) into our periodic solution (31), and using the constraint condition $e_0 = \sqrt{\frac{g_2(T)}{12}}$ derived from the consistency relation between the Weierstrass invariants $g_2(T)$, $g_3(T)$, and the parameters e_0, $\gamma(T)$ under the condition that the discriminant is zero, and using the hyperbolic function identity $\sinh^2 x = \cosh^2 x - 1$

$$A(x,t) = \frac{6G_1}{\Omega(\varepsilon^{9/2}t) + e_5(\varepsilon^{9/2}t)k} \cdot \frac{1 - \operatorname{sech}^2\left[\sqrt{\dfrac{3g_2(\varepsilon^{9/2}t)}{4}}\left(k(x - c_0 t) + \varepsilon^{9/2}\int \Omega(\varepsilon^{9/2}t)\,\mathrm{d}t - \zeta_0\right)\right]}{2 - \operatorname{sech}^2\left[\sqrt{\dfrac{3g_2(\varepsilon^{9/2}t)}{4}}\left(k(x - c_0 t) + \varepsilon^{9/2}\int \Omega(\varepsilon^{9/2}t)\,\mathrm{d}t - \zeta_0\right)\right]}, \tag{33}$$

where

$$g_2(\varepsilon^{9/2}t) = \frac{G_1 e_4(\varepsilon^{9/2}t)}{6e_1(\varepsilon^{9/2}t)^2 k^5} + \frac{[\Omega(\varepsilon^{9/2}t) + e_5(\varepsilon^{9/2}t)k]^2}{12e_1(\varepsilon^{9/2}t)^2 k^6}. \tag{34}$$

The periodic solution (31) is obtained under the assumption $\alpha = 0$, which corresponds to the weak nonlinearity approximation where the quartic nonlinear effect is relatively weak (i.e., $|e_2| \ll 1$). Under this approximation, both the periodic solution and its degenerate solitary wave counterpart Eq. (33) correspond to the variable-coefficient cubic KdV model, i.e., the case where the quartic nonlinear term can be treated as a higher-order small quantity. This approximation is physically justified when the wave amplitude is moderate, the background flow variations are gradual, or the higher-order nonlinear effects are subdominant. Under these conditions, the solitary wave solution (33) effectively captures the essential features of Rossby wave evolution in time-dependent background flows, including amplitude modulation, phase shift, and structural stability.

It is important to emphasize that the solitary wave solution (33) is obtained under the weak nonlinearity approximation (i.e., $|e_2| \ll 1$) and does not incorporate the full quartic nonlinearity of the original vfqKdV equation. Nevertheless, it provides a solid analytical foundation for understanding wave-mean flow interactions in weakly nonlinear regimes. For situations where the quartic nonlinear effect becomes significant (i.e., $|e_2|$ is not small), a more general solution method is required, which we leave for future investigation. In the following sections, we adopt the solitary wave solution (33) as the basis for parametric analysis and numerical simulations, focusing on its physical implications under the weak nonlinearity approximation.

4. Results and discussion

Finally, the full stream function solution, incorporating both the background flow and the finite-amplitude wave disturbance, is reconstructed as

$$\psi = b_0 \sin\left(\frac{\pi y}{y_0}\right) - b_1 y + \varepsilon\left(a_1 y^2 + a_2(t) y + a_3(t)\right) + \varepsilon \sin\left(\frac{\pi y}{y_0}\right) \left\{ \frac{6G_1}{\Omega(\varepsilon^{9/2}t) + e_5(\varepsilon^{9/2}t)k} \frac{1 - \operatorname{sech}^2\left[\sqrt{\frac{3g_2(\varepsilon^{9/2}t)}{4}}\left(k(x - c_0 t) + \varepsilon^{9/2}\int \Omega(\varepsilon^{9/2}t)\,\mathrm{d}t - \zeta_0\right)\right]}{2 - \operatorname{sech}^2\left[\sqrt{\frac{3g_2(\varepsilon^{9/2}t)}{4}}\left(k(x - c_0 t) + \varepsilon^{9/2}\int \Omega(\varepsilon^{9/2}t)\,\mathrm{d}t - \zeta_0\right)\right]} \right\}. \tag{35}$$

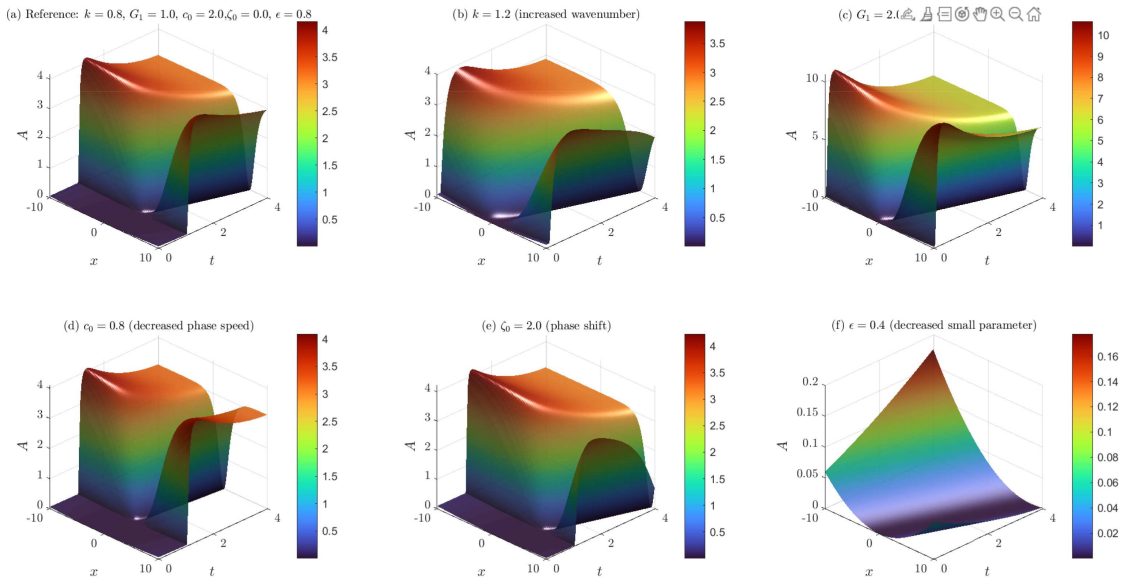


Fig. 1. Effects of different parameters on the solitary wave solution.

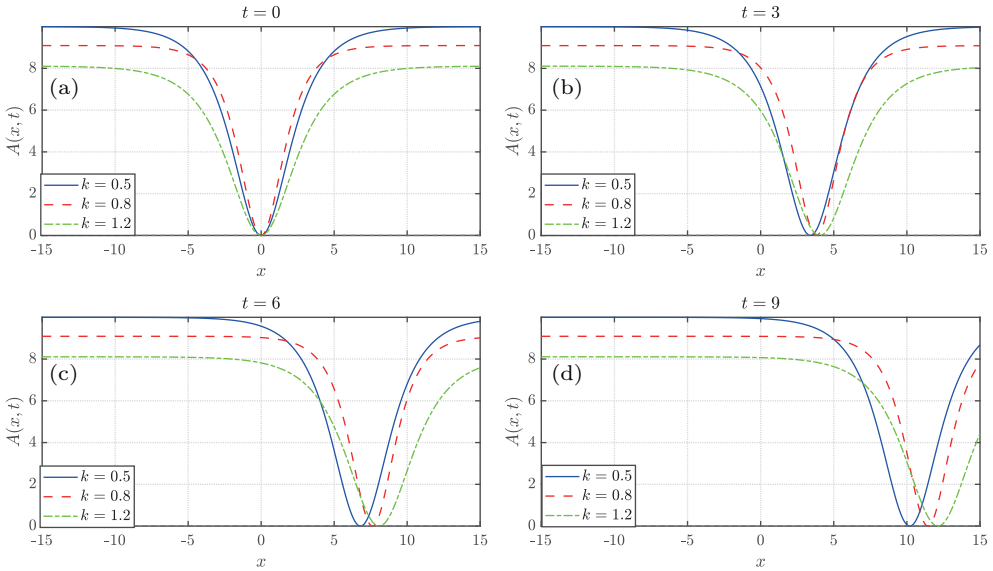


Fig. 2. Variation of amplitude A under different values of t, with $G_1 = 2.0$, $\zeta_0 = 0.0$, $c_0 = 1.5$, $\varepsilon = 0.8$.

Based on the derived vfqKdV model and the exact solitary wave solution given by Eq. (35), we systematically investigate the evolution characteristics of nonlinear Rossby waves under a time-dependent background flow. Numerical simulations are carried out to elucidate the influence of key physical parameters on wave amplitude, phase speed, and spatial structure, with particular attention to the modulation effects of the time-varying background flow.

Figure 1 illustrates the effects of key parameters on the solitary wave profile in a three-dimensional space-time representation. Figure 1(a) shows the reference case with $k = 0.8$, $G_1 = 1.0$, $c_0 = 2.0$, and $\varepsilon = 0.8$, exhibiting a standard bell-shaped solitary wave. As shown in Fig. 1(b), increasing the wavenumber to $k = 1.2$ results in a narrower waveform, indi-

cating enhanced localization of wave energy. A larger integration constant $G_1 = 2.0$ (Fig. 1(c)) amplifies the wave amplitude linearly, consistent with the analytical relation $A \propto G_1$ derived from Eq. (35). Reducing the phase speed to $c_0 = 0.8$ (Fig. 1(d)) slows down the eastward propagation of the wave packet without affecting the amplitude or shape. Increasing the phase constant to $\zeta_0 = 2.0$ (Fig. 1(e)) shifts the initial position of the solitary wave to the right, reflecting the translational invariance of the system. Finally, decreasing the small parameter to $\varepsilon = 0.4$ (Fig. 1(f)) reduces the overall wave amplitude, demonstrating that ε modulates the strength of nonlinearity.

Figure 2 displays the spatial distribution of the amplitude $A(x,t)$ for three different wavenumbers $k = 0.5, 0.8, 1.2$ at four distinct times $t = 0, 3, 6, 9$, with $G_1 = 2.0$ and $c_0 = 1.5$. For each fixed wavenumber, the waveform retains its shape as time evolves, with the peak position shifting uniformly to the right. This confirms that under constant background coefficients, the solitary wave propagates steadily without amplitude decay or shape distortion, demonstrating structural stability. Moreover, the waveform becomes narrower as k increases, indicating that the wavenumber controls the wave width while leaving the peak amplitude unchanged.

Figure 3 illustrates the effect of the integration constant G_1 on the solitary wave profile. The amplitude distributions are shown for three different values $G_1 = 1.8, 2.0, 2.2$ at four distinct times $t = 0, 3, 6, 9$, with the wavenumber fixed at $k = 0.8$ and $c_0 = 1.5$. For each fixed G_1, the waveform retains its shape as time evolves, with the peak position shifting uniformly to the right, confirming the structural stability of the solitary wave. The peak amplitude increases linearly with G_1, consistent with the analytical relation $A \propto G_1$ derived from Eq. (35). Meanwhile, the waveform width remains unchanged, indicating that G_1 modulates the amplitude independently of the spatial scale.

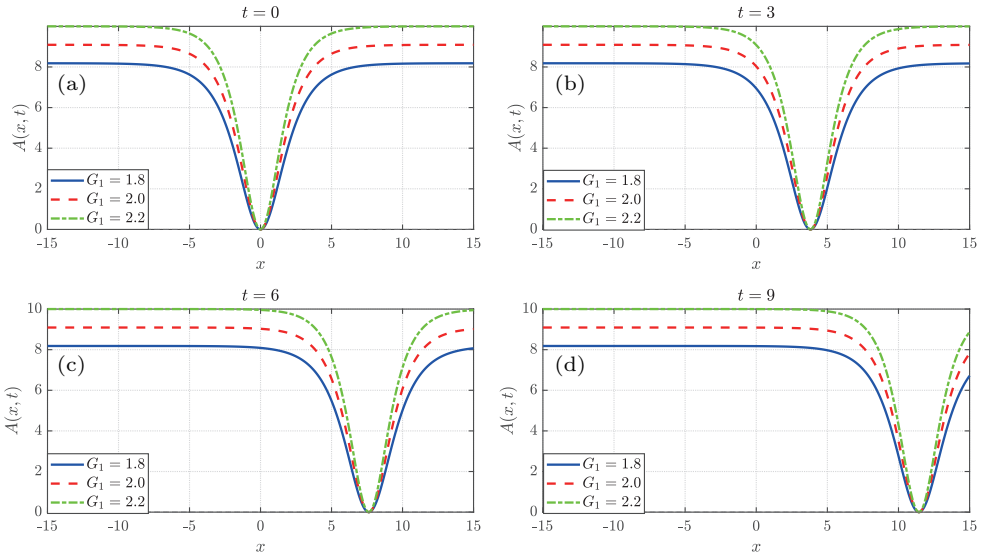


Fig. 3. Variation of amplitude A under different values of t, with $k = 0.8$, $\zeta_0 = 0.0$, $c_0 = 1.5$, $\varepsilon = 0.8$.

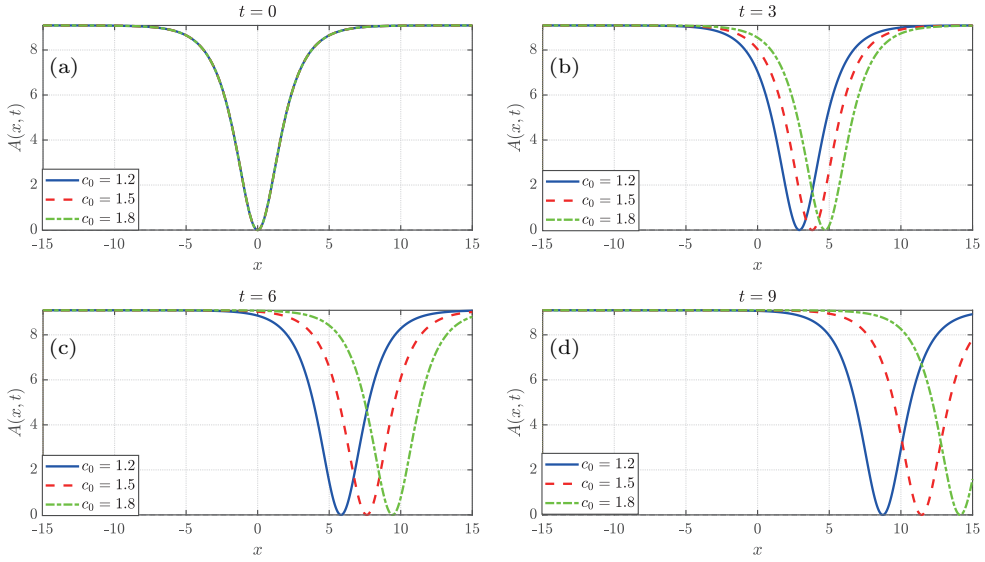


Fig. 4. Variation of amplitude A under different values of t, with $G_1 = 2.0$, $k = 0.8$, $\zeta_0 = 0.0$, $\varepsilon = 0.8$.

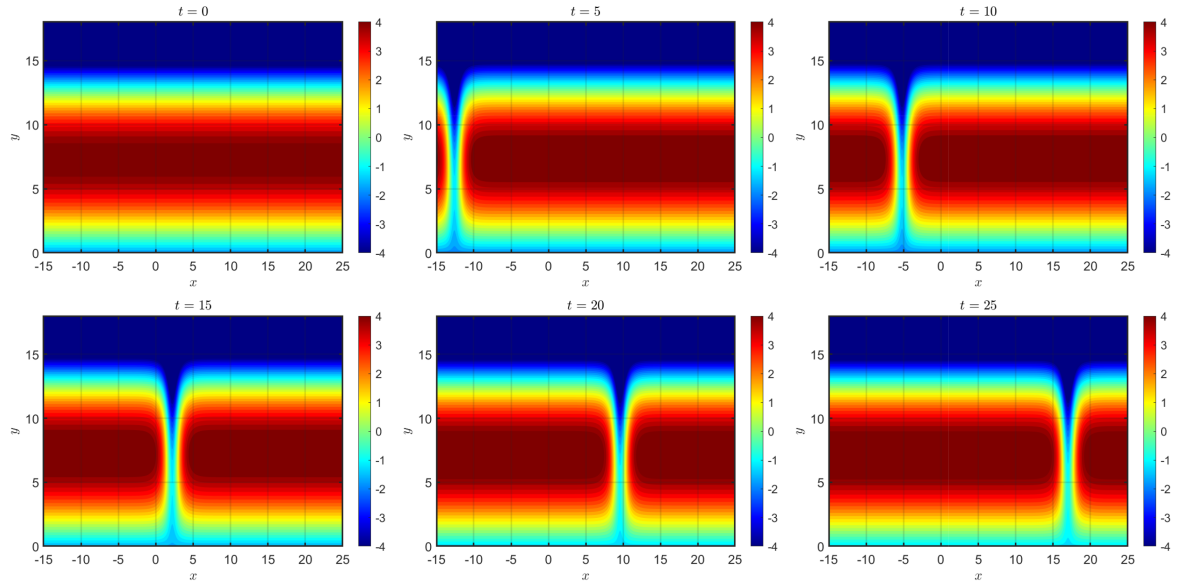


Fig. 5. The contour plot of the flow field with $b_0 = 5.0$, $b_1 = 0.7$, $a_1 = 0.02$, $a_2 = 0.1\sin(0.2t)$, $a_3 = 0.05\cos(0.2t)$, $G_1 = 3.0$, $k = 0.4$, $c_0 = 1.5$, $\varepsilon = 0.4$, $y_0 = 18.0$, $\zeta_0 = -8.0$.

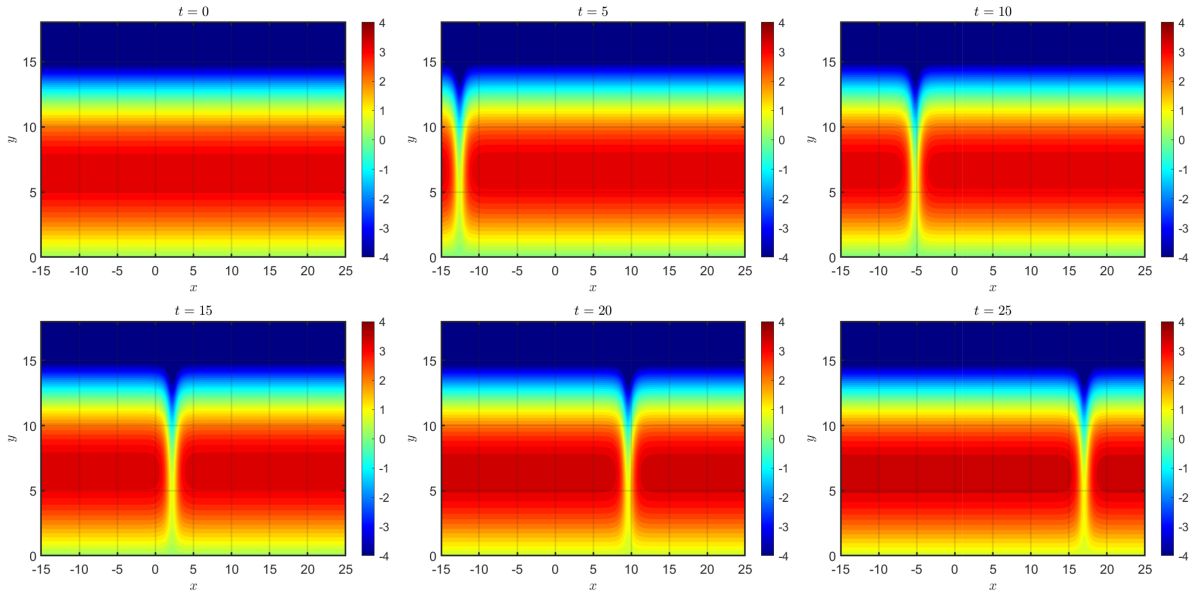


Fig. 6. The contour plot of the flow field with $b_0 = 5.0$, $b_1 = 0.7$, $a_1 = 0.02$, $a_2 = 0.1\sin(0.2t)$, $a_3 = 0.05\cos(0.2t)$, $G_1 = 1.5$, $k = 0.4$, $c_0 = 1.5$, $\varepsilon = 0.4$, $y_0 = 18.0$, $\zeta_0 = -8.0$.

Figure 4 demonstrates the influence of the phase speed c_0 on the propagation of the solitary wave. The amplitude distributions are plotted for three different values of $c_0 = 1.2, 1.5, 1.8$ at four distinct times $t = 0, 3, 6, 9$, with the wavenumber fixed at $k = 0.8$ and $G_1 = 2.0$. At the initial time $t = 0$, the waveforms for different c_0 coincide, reflecting identical initial conditions. As time progresses, the wave packets separate: larger c_0 results in a faster eastward shift of the peak position, while the waveform shape and peak amplitude remain unchanged. The propagation speed extracted from the numerical simulations matches the theoretical value c_0, validating the correctness of the solution. This confirms that c_0 governs the translational motion of the solitary wave without affecting its amplitude or spatial structure.

Figures 5–8 present contour plots of the reconstructed stream function $\psi(x, y, t)$ at six consecutive time instants $t = 0, 5, 10, 15, 20, 25$, revealing the formation and propagation of well-defined vortical structures. Figure 5 shows the case with $G_1 = 3.0$, $\zeta_0 = -8$, and channel width $y_0 = 18$. A coherent anticyclonic vortex emerges and propagates eastward, maintaining its structural integrity over time. Reducing the integration constant to $G_1 = 1.5$ (Fig. 6) results in a weaker vortex with reduced amplitude, further confirming the amplitude-modulating role of G_1. Adjusting the phase constant to $\zeta_0 = -4$ (Fig. 7) shifts the initial position of the vortex eastward without altering its shape, consistent with the phase invariance property of solitary waves. Changing the channel width to $y_0 = 10$ (Fig. 8) compresses the vortex in the meridional

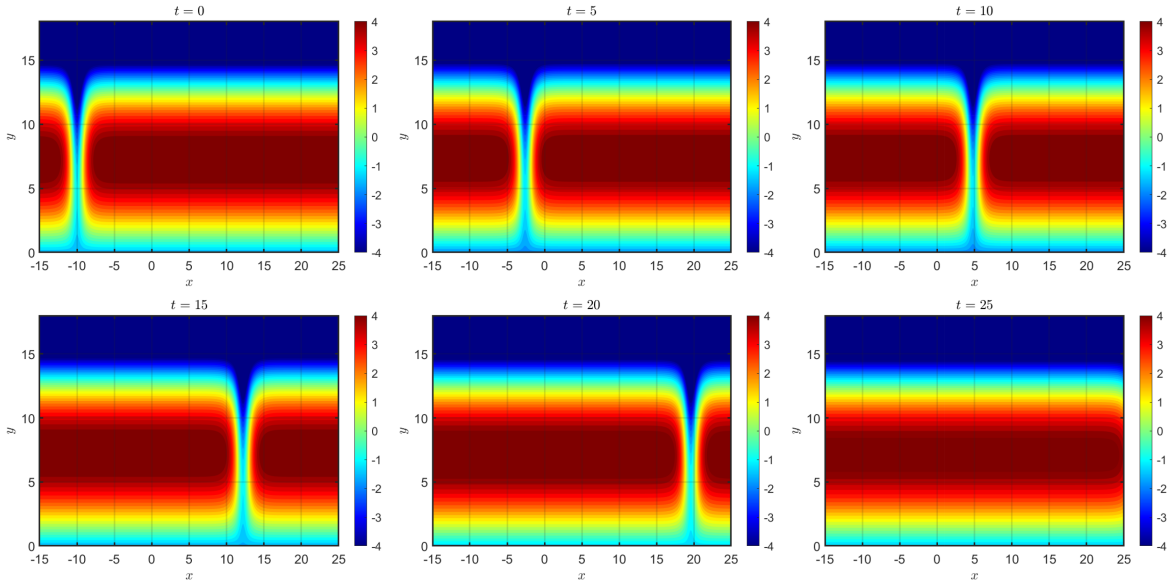


Fig. 7. The contour plot of the flow field with $b_0 = 5.0$, $b_1 = 0.7$, $a_1 = 0.02$, $a_2 = 0.1\sin(0.2t)$, $a_3 = 0.05\cos(0.2t)$, $G_1 = 3.0$, $k = 0.4$, $c_0 = 1.5$, $\varepsilon = 0.4$, $y_0 = 18.0$, $\zeta_0 = -4.0$.

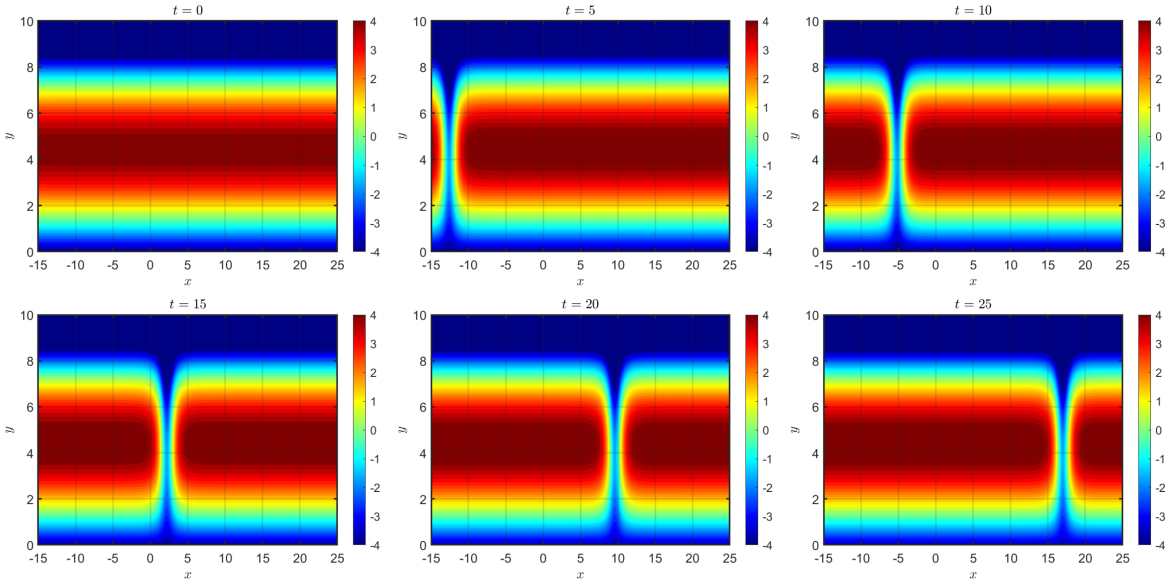


Fig. 8. The contour plot of the flow field with $b_0 = 5.0$, $b_1 = 0.7$, $a_1 = 0.02$, $a_2 = 0.1\sin(0.2t)$, $a_3 = 0.05\cos(0.2t)$, $G_1 = 3.0$, $k = 0.4$, $c_0 = 1.5$, $\varepsilon = 0.4$, $y_0 = 10.0$, $\zeta_0 = -8.0$.

direction, leading to stronger localization of the flow structure and enhanced energy density. This demonstrates that the channel width significantly influences the meridional structure of the vortex, while the horizontal propagation remains unaffected.

The numerical results presented in Figs. 1–8 collectively validate the correctness of the derived solitary wave solution and reveal the key roles of the governing parameters. Under the weak nonlinearity approximation adopted in this study, the quartic nonlinear term $e_2A^3A_X$ is treated as a higher-order small quantity; nevertheless, the time-dependent background flow, captured by the variable coefficients $e_i(T)$, still plays a dominant role in modulating the wave amplitude, width, and phase speed.

The variable-coefficient quartic KdV model derived in this study incorporates a quartic nonlinear term $e_2A^3A_X$. The analytical solution presented herein is obtained under the weak nonlinearity approximation, where the quartic nonlinear effect is relatively weak (i.e., $|e_2| \ll 1$), corresponding to the case in which the quartic nonlinear term can be treated as a higher-order small quantity. This approximation is physically justified when the Rossby wave amplitude is sufficiently small, the background shear is weak, or the topographic variations are gentle. Under these conditions, the cubic nonlinearity $e_3A^2A_X$ and quadratic nonlinearity e_4AA_X dominate the wave dynamics. Nevertheless, the derived solitary wave solution reveals that, even under this weak nonlinearity approximation, the time-dependent background flow, captured by the variable coefficients $e_i(T)$, significantly modulates the wave amplitude, width, and phase speed. For situations where the quartic non-

linear effect becomes significant (e.g., large-amplitude waves or strongly sheared backgrounds), the present solution may serve as a limiting case, and a more comprehensive analysis incorporating the full quartic nonlinearity is warranted.

5. Conclusion

In this study, we have systematically investigated the evolution of nonlinear Rossby waves in a dynamically time-dependent background flow using a vfqKdV-type model. Starting from the quasi-geostrophic potential vorticity conservation equation under the β-plane approximation and employing the Gardner–Morikawa transformation combined with multi-scale perturbation analysis, we derived a vfqKdV equation with explicit time-dependent coefficients. This model generalizes existing constant-coefficient or lower-order nonlinear formulations and effectively captures the influence of spatiotemporal variations in the background flow.

An exact periodic traveling wave solution was constructed using a fractional linear transformation based on the Weierstrass elliptic function under the weak nonlinearity approximation, where the quartic nonlinear effect is relatively weak (i.e., $|e_2| \ll 1$). By applying the degeneracy condition $\Delta = 0$, the periodic solution reduces to a solitary wave solution. This solitary wave solution corresponds to the case where the quartic nonlinear term can be treated as a higher-order small quantity — a physically plausible approximation for weakly nonlinear Rossby waves in gradually varying background flows. The solution reveals that the wave amplitude and phase are modulated by time-dependent background parameters.

Numerical simulations were conducted to examine the sensitivity of the wave structure to key parameters such as wavenumber k, integration constant G_1, phase speed c_0, and phase constant ζ_0. The results demonstrate that the time-dependent background flow significantly modulates the wave amplitude, width, and phase speed, even under the weak nonlinearity approximation. The amplitude scales linearly with G_1 and remains stable under constant background conditions. The wavenumber k controls the width of the solitary wave, with larger k yielding narrower profiles. The phase speed c_0 dictates the translation velocity, while ζ_0 determines the initial position. These findings confirm the structural stability and parameter sensitivity of the derived solitary wave solution. The reconstructed stream function further illustrates the formation of eastward-propagating vortical structures, whose strength and position are modulated by the background flow and nonlinear parameters. These results provide a theoretical basis for understanding complex wave phenomena such as atmospheric blocking and oceanic eddy genesis.

In conclusion, the variable-coefficient quartic KdV model established in this study, together with its solitary wave solution obtained under the weak nonlinearity approximation, offers a robust and physically meaningful framework for studying finite-amplitude Rossby waves in non-stationary geophysical flows. The solution reveals how time-dependent background flows modulate the amplitude, width, and propagation of Rossby solitary waves. For strongly nonlinear regimes where the quartic nonlinear effect cannot be neglected, the present work provides a foundation for further investigation.

Appendix A

$$
\begin{aligned}
I_0 &= \int_0^{y_0} \frac{\partial^2 G_1}{\partial y^2}\,\mathrm{d}y = \left.\frac{\partial G_1}{\partial y}\right|_0^{y_0},\\
I_1 &= \int *0^{y_0} \left(-\frac{dU_0}{\mathrm{d}y} G_1\right)\mathrm{d}y,\\
I_2 &= \int_0^{y_0} \left(\frac{1}{3} G_1 \frac{\partial^3 G_{33}}{\partial y^3} + \frac{1}{2} G_{22} \frac{\partial^3 G_{22}}{\partial y^3} + \frac{\partial^2 G_{33}}{\partial y^2}\frac{\partial^3 G_1}{\partial y^3}\right.\\
&\quad \left. -\frac{1}{3}\frac{\partial^2 G_1}{\partial y^2}\frac{\partial G_{32}}{\partial y} - \frac{1}{2}\frac{\partial^2 G_{22}}{\partial y^2}\frac{\partial G_{22}}{\partial y} - \frac{\partial^2 G_{33}}{\partial y^2}\frac{\partial G_1}{\partial y}\right)\mathrm{d}y,\\
I_3 &= \int_0^{y_0} \left(G_{33}\frac{\partial^3 U_1}{\partial y^3} + \frac{1}{2} G_1 \frac{\partial^3 G_{32}}{\partial y^2} + \frac{1}{2} G_{21}\frac{\partial^3 G_{22}}{\partial y^3}\right.\\
&\quad + G_{22}\frac{\partial^3 G_{21}}{\partial y^3} + \frac{\partial^3 G_{32}}{\partial y^2}\frac{\partial^3 G_1}{\partial y^3} - \frac{\partial^3 G_{33}}{\partial y^2}\frac{\partial U_1}{\partial y}\\
&\quad - \frac{1}{2}\frac{\partial^2 G_1}{\partial y^2}\frac{\partial G_{32}}{\partial y} - \frac{1}{2}\frac{\partial^2 G_{21}}{\partial y^2}\frac{\partial G_{22}}{\partial y}\\
&\quad \left. - \frac{\partial^2 G_{22}}{\partial y^2}\frac{\partial G_{21}}{\partial y} + \frac{\partial^2 G_{32}}{\partial y^2}\frac{\partial G_1}{\partial y}\right)\mathrm{d}y,\\
I_4 &= \int_0^{y_0} \left(G_{22}\frac{\partial^3 U_2}{\partial y^3} + G_{32}\frac{\partial^3 U_1}{\partial y^3} + G_1\frac{\partial^3 G_{31}}{\partial y^3}\right.\\
&\quad + \frac{\partial^2 G_{31}}{\partial y^2}\frac{\partial^3 G_1}{\partial y^3} - \frac{\partial^2 G_{32}}{\partial y^2}\frac{\partial U_1}{\partial y} - \frac{\partial^2 G_{22}}{\partial y^2}\frac{\partial U_2}{\partial y}\\
&\quad \left. - \frac{\partial^2 G_1}{\partial y^2}\frac{\partial G_{31}}{\partial y} - \frac{\partial^2 G_{21}}{\partial y^2}\frac{\partial G_{21}}{\partial y} - \frac{\partial^2 G_{21}}{\partial y^2}\frac{\partial G_1}{\partial y}\right)\mathrm{d}y,\\
I_5 &= \int_0^{y_0} \left(G_1\frac{\partial^3 U_3}{\partial y^3} + G_{21}\frac{\partial^3 U_2}{\partial y^3} + G_{31}\frac{\partial^3 U_1}{\partial y^3}\right.\\
&\quad \left. - \frac{\partial^2 G_1}{\partial y^2}\frac{\partial U_3}{\partial y} - \frac{\partial^2 G_{21}}{\partial y^2}\frac{\partial U_2}{\partial y} - \frac{\partial^2 G_{31}}{\partial y^2}\frac{\partial U_1}{\partial y}\right)\mathrm{d}y,\\
I_6 &= \int_0^{y_0} \frac{\partial^3 G_1}{\partial T\,\partial y^2}\,\mathrm{d}y = \left.\frac{\partial^2 G_1}{\partial T\,\partial y}\right|_0^{y_0},\\
I_7 &= \int_0^{y_0} \frac{\partial^3 U_1}{\partial T\,\partial y^2}\,\mathrm{d}y = \left.\frac{\partial^2 U_1}{\partial T\,\partial y}\right|_0^{y_0},\\
C_0 &= A_5\beta^5 + A_4\beta^4 + A_3\beta^3 + A_2\beta^2 + A_1\beta + A_0,\\
C_1 &= 5A_5\alpha\beta^4 + A_4(\beta^4\gamma + 4\alpha\beta^3) + A_3(3\alpha\beta^2 + 2\beta^3\gamma)\\
&\quad + A_2(2\alpha\beta + 3\beta^2\gamma) + A_1(\alpha + 4\beta\gamma) + 5A_0\gamma,\\
C_2 &= 10A_5\alpha^2\beta^3 + A_4(4\alpha\beta^3\gamma + 6\alpha^2\beta^2)\\
&\quad + A_3(3\alpha^2\beta + 6\alpha\beta^2\gamma + \beta^3\gamma^2)\\
&\quad + A_2(\alpha^2 + 6\alpha\beta\gamma + 3\beta^2\gamma^2)
\end{aligned}
$$

$$
\begin{aligned}
&+A_1(4\alpha\gamma+6\beta\gamma^2)+10A_0\gamma^2,\\
C_3 &= 10A_5\alpha^3\beta^2+A_4(6\alpha^2\beta^2\gamma+4\alpha^3\beta)\\
&+A_3(\alpha^3+6\alpha^2\beta\gamma+3\alpha\beta^2\gamma^2)\\
&+A_2(3\alpha^2\gamma+6\alpha\beta\gamma^2+\beta^2\gamma^3)\\
&+A_1(6\alpha\gamma^2+4\beta\gamma^3)+10A_0\gamma^3,\\
C_4 &= 5A_5\alpha^4\beta+A_4(4\alpha^3\beta\gamma+\alpha^4)+A_3(3\alpha^2\beta\gamma^2+2\alpha^3\gamma)\\
&+A_2(2\alpha\beta\gamma^3+3\alpha^2\gamma^2)+A_1(\beta\gamma^4+4\alpha\gamma^3)+5A_0\gamma^4,\\
C_5 &= A_5\alpha^5+A_4\alpha^4\gamma+A_3\alpha^3\gamma^2+A_2\alpha^2\gamma^3+A_1\alpha\gamma^4+A_0\gamma^5.
\end{aligned}
$$

Acknowledgments

Project supported by the National Natural Science Foundation of China (Grant Nos. 12462021, 12102205, and 12262025), the Central Guidance for Local Scientific and Technological Development Funding Projects (Grant No. 2024ZY0117), the Outstanding Youth Science Fund Project of the Natural Science Foundation of Inner Mongolia Autonomous Region of China (Grant No. 2025JQ006), the Program for Talent Revitalization of Inner Mongolia Team (Grant No. 2025TEL06), the Program for Young Talents of Science and Technology in Universities of Inner Mongolia Autonomous Region of China (Grant No. NJYT23098), and the Scientific Starting and the Innovative Research Team in the Universities of Inner Mongolia Autonomous Region of China (Grant No. NMGIRT2208).

References

[1] Rossby C G 1939 *J. Mar. Res.* **2** 38
[2] Hoskins B J and Karoly D J 1981 *J. Atmos. Sci.* **38** 1179
[3] Pedlosky J 2013 *Geophysical Fluid Dynamics* (New York: Springer) pp. 1
[4] Gill A E 2016 *Atmosphere–Ocean Dynamics* (Amsterdam: Elsevier) pp. 1
[5] Longuet-Higgins H C 1964 *Proc. R. Soc. Lond. A* **279** 446
[6] Zabusky N J and Kruskal M D 1965 *Phys. Rev. Lett.* **15** 240
[7] Benney D J 1966 *J. Math. Phys.* **45** 52
[8] Rhines P B 1975 *J. Fluid Mech.* **69** 417
[9] Williams G P 1978 *J. Atmos. Sci.* **35** 1399
[10] Vallis G K 2017 *Atmospheric and Oceanic Fluid Dynamics* (Cambridge: Cambridge University Press) pp. 1
[11] Zhang Z, Zhang R, Wang J and Yang L 2023 *Nonlinear Dyn.* **111** 17483
[12] Wang J, Zhang R and Yang L 2020 *Phys. Fluids* **32** 096602
[13] Redekopp L G 1977 *J. Fluid Mech.* **82** 725
[14] Ono H 1975 *J. Phys. Soc. Jpn.* **39** 1082
[15] Johnson R S 1997 *A Modern Introduction to the Mathematical Theory of Water Waves* (Cambridge: Cambridge University Press) pp. 19
[16] Grimshaw R, Guo C, Helfrich K and Vlasenko V 2014 *J. Phys. Oceanogr.* **44** 1116
[17] Ablowitz M J and Segur H 1981 *Solitons and the Inverse Scattering Transform* (Philadelphia: Society for Industrial and Applied Mathematics) pp. 25
[18] Rogers C and Shadwick W F 1982 *Bäcklund Transformations and Their Applications* (New York: Academic Press) pp. 30
[19] Hirota R 2004 *The Direct Method in Soliton Theory* (Cambridge: Cambridge University Press) pp. 155
[20] Liu S, Fu Z, Liu S and Zhao Q 2001 *Phys. Lett. A* **289** 69
[21] Fan E 2000 *Phys. Lett. A* **277** 212
[22] Bender C M and Orszag S A 2013 *Advanced Mathematical Methods for Scientists and Engineers I: Asymptotic Methods and Perturbation Theory* (New York: Springer) pp. 10
[23] Liu W X, Dao L G and Zhang R G 2025 *Chin. Phys. B* **34** 070504
[24] Jia Y H, Wang D L, Shen B, Ju Z T, Huang Q Y, Wang X P, Zhang J H, Liu W, Wang Y Y and Dai C Q 2026 *Laser Photonics Rev.* **20** 2503212
[25] Jia Y H, Si Z Z, Ju Z T, Feng H Y, Zhang J H, Yan X and Dai C Q 2025 *Sci. China Phys. Mech. Astron.* **68** 284211
[26] Huang L, Wang D S and Zhu X 2026 *Math. Ann.* **395** 18
[27] Jin X W, Shen S J, Yang Z Y and Lin J 2022 *Phys. Rev. E* **105** 014205
[28] Jin X W and Lin J 2020 *J. Magn. Magn. Mater.* **502** 166590
[29] Mou D S, Si Z Z, Qiu W X and Dai C Q 2025 *Opt. Laser Technol.* **181** 111774
[30] Si Z Z, Wang D L, Zhu B W, Ju Z T, Wang X P, Liu W, Malomed B A, Wang Y Y and Dai C Q 2024 *Laser Photonics Rev.* **18** 2400097
[31] Wang D, Liu Z, Zhao H, Qin H, Bai G, Chen C, Wan J, Liu Z and Dai C 2025 *Science* **389** 935
[32] Boyd J P 1980 *J. Phys. Oceanogr.* **10** 1699
[33] Pedlosky J 1970 *J. Atmos. Sci.* **27** 15
[34] Charney J G 1949 *J. Atmos. Sci.* **6** 371
[35] Whittaker E T and Watson G N 1996 *A Course of Modern Analysis* (4th edn.) (Cambridge: Cambridge University Press) pp. 45
[36] Byrd P F and Friedman M D 1971 *Handbook of Elliptic Integrals for Engineers and Scientists* (2nd edn.) (Berlin: Springer) pp. 12
[37] Zakharov V E 1968 *J. Appl. Mech. Tech. Phys.* **9** 190
[38] Majda A 2003 *Introduction to PDEs and Waves for the Atmosphere and Ocean* (Providence: American Mathematical Society) pp. 9
[39] Salmon R 1998 *Lectures on Geophysical Fluid Dynamics* (Oxford: Oxford University Press) pp. 15
[40] Hou S, Zhang R, Zhang Z and Yang L 2024 *Wave Motion* **124** 103249
[41] Grimshaw R 1984 *Annu. Rev. Fluid Mech.* **16** 11
[42] Whittaker E T and Watson G N 2020 *A Course of Modern Analysis* (Cambridge: Cambridge University Press) pp. 55
[43] Abramowitz M and Stegun I A 1964 *Handbook of Mathematical Functions with Formulas, Graphs, and Mathematical Tables* (Washington, D.C.: National Bureau of Standards) pp. 651